Fragmentation Pathways of $[Mg(NH_3)_n]^{2+}$ Complexes: Electron Capture versus Charge Separation†

Bohan Wu, Bridgette J. Duncombe, and Anthony J. Stace*

Department of Physical Chemistry, School of Chemistry, The University of Nottingham, University Park, Nottingham NG7 2RD, U.K.

Received: December 16, 2005; In Final Form: March 7, 2006

New experimental results are presented from a detailed study of gas-phase $[Mg(NH_3)_n]^{2+}$ complexes and their fragmentation pathways. The reactions examined range from those observed as metastable (unimolecular) decompositions through to collision-induced processes, which have been accessed using a variety of collision gases. Measurements of ion intensity distributions coupled with unimolecular decay studies show that $[Mg(NH_3)_4]^{2+}$ not only is the most intense species detected but also sits at a critical boundary between complexes that are unstable with respect to charge separation and those that are sufficiently solvated to be deemed stable on the time scale of the experiment. Metastable fragmentation patterns have been used to provide information on the evolution of solvent structure around the central dication. In addition to highlighting the particular significance of $[Mg(NH_3)_4]^{2+}$, these measurements show some evidence to suggest the buildup of structures via a hydrogen-bonded network to give conformers of the form (4+1) and (4+2), respectively. Collision-induced dissociation studies show the ions to exhibit several fragmentation pathways, including the loss of NH_3 and NH_3 + H, which are promoted primarily through electron capture dissociation (ECD). This picture contrasts with the conclusion from a number of earlier studies that collisional activation mainly promotes charge separation. From the results presented it is suggested that electron capture may play a more dominant role in the charge reduction of multiply charged metal−ligand species than had previously been appreciated.

Introduction

Much of the current interest in the behavior of gas-phase multiply charged metal−ligand complexes has centered on their reactivity following collisional activation.[1] Excitation of the ions is frequently accompanied by charge reduction on the part of the metal cation, and the accepted interpretation of such events is that they arise as a result of either internal electron transfer from a ligand to the metal or proton transfer between ligands in the case of protic solvents.[1−10] As a consequence of charge transfer, Coulomb repulsion usually causes the complex to break up, giving charged fragments with high center-of-mass kinetic energies.[7−10] The potential energy required to drive this repulsion is derived from the difference between the first ionization energy of a typical ligand ∼10 eV and the second ionization energy of a metals ∼15 eV. From the point of view of a collision between a doubly charged metal cation and a neutral ligand, it is energetically more favorable to transfer charge than to form a stable complex. Weisshaar et al.[11,12] have modeled such an encounter, which enabled them to distinguish between direct charge-transfer and charge reduction accompanied by chemical reactivity. There are several recent reviews that provide an introduction to the study of multiply charged ions in the gas-phase.[13,14]

The fragmentation of a multiply charged metal−ligand complex can be seen as the reverse of the process first described by Tonkyn and Weisshaar.[11] Between the potential well of the stable $[M{\cdot}L_n]^{m+}$ entity and the $[M{\cdot}L_{n-1}]^{m+}$ + L asymptote lie several curve crossing points that, at their simplest, pass through to $[M{\cdot}L_{n-1}]^{(m-1)+}$ + L^+ as electron-transfer products but can involve encounters with more complex chemical processes. Quite often, the energetics of formation of reaction products, such as MOH^+, are sufficiently favorable that the products of bond-breaking processes are the dominant fragment ions. In terms of curve crossing processes, what is encountered first on the incoming collision channel is likely to be least probable on the outgoing decay path of a complex.

Given the range of possible decay pathways open to a multiply charged metal−ligand complex, there are certain anomalies associated with experimental observations following their collisional excitation. First, in some of the examples studied at high collision energies,[7−10] a significant fraction of the nonmetallic ion signal appears to be absent and second, many charged fragments emerge with quite modest (∼0.2 eV) kinetic energies, even though the potential energy difference between the two charged states (approximately second IE of the metal minus the first IE of the ligand) can be >5 eV.[10] The absence of nonmetallic cations can, in part, be explained by the lighter ions acquiring a larger fraction of the kinetic energy release and, therefore, being scattered out of the flight path to the detector. The reduced kinetic energy could be attributed to a high degree of internal excitation as a result of the shape of the potential energy surface on which the fragments emerge.

Presented here are the results of a detailed experimental study undertaken on the $[Mg(NH_3)_n]^{2+}$ system. Measurements have been made of the decay patterns of the ions during metastable (unimolecular) decay and following collisional activation. The results show the presence of a competition between charge separation and electron capture from the collision gas with the latter becoming the dominant charge reduction mechanism in larger complexes. As might be expected, electron capture is also found to be sensitive to the nature of the collision gas. A limited

† Part of the "Chava Lifshitz Memorial Issue".

10.1021/jp0573442 CCC: $33.50
Published on Web 04/04/2006

study of $[Mg(NH_3)_n]^{2+}$ complexes has been undertaken earlier in this laboratory;[9] however, improvements in sensitivity and energy resolution make it necessary to modify some of our earlier conclusions. Overall, there is a marked lack of experimental data on $[Mg(NH_3)_n]^{2+}$ complexes; this is in contrast to the singly charged $[Mg(NH_3)_n]^+$ series, which has been investigated thoroughly using a number of experimental and theoretical techniques.[15−19] For the $[Mg(NH_3)_n]^+$ system, calculations and collision-induced dissociation studies show that ammonia ligates directly to the central magnesium cation at small values of *n*; however, as *n* increases, the propensity to hydrogen bond increases such that for $n = 3-5$ isomers exist.[15−17] Photodissociation spectra and ab initio studies of small $[Mg(NH_3)_n]^+$ species by Fuke and co-workers[18,19] have shown that photoinduced charge transfer and intracluster reactions dominate at small values of *n*, with ions such as $[MgNH_2]^+$, NH_3^+ and even Mg^+ being generated. Such behavior is analogous to small $[Mg(H_2O)_n]^+$ complexes, where the products of H atom loss such as hydrated $[MgOH]^+$, are seen.[20,21]

Experimental Section

The experimental apparatus used for generation, identification and detection of gas-phase multiply charged metal−ligand complexes has been described extensively in previous publications.[9,10,22] Briefly, the first step is to produce mixed neutral clusters by adiabatic expansion through a pulsed supersonic nozzle of a 1% ammonia/argon gas mix (BOC speciality gases). Neutral clusters of varying composition including Ar_m, $Ar_m(NH_3)_n$, and $(NH_3)_n$, then pass through a region where magnesium vapor ($\sim 10^{-2}$ mbar) is generated by a Knudsen effusion cell (DCA Instruments, EC-40-63-21) operating at 470 °C. Neutral magnesium atoms collide with the molecular beam of clusters to produce various neutral clusters including some with the form $Mg.Ar_m(NH_3)_n$. Del Mistro and Stace[23] have shown with a molecular dynamics simulation that in the simpler case of colliding Ar_{20} with a single acetonitrile molecule, the cluster first melts and the molecule then moves below the surface within 40 ps of the collision; the mixed cluster then achieves stabilization through the evaporation of argon. It is quite clear for these experiments that argon atom evaporation is an essential part of the "pick-up" and facilitates the dispersion of energy on addition of a metal atom and after electron impact ionization.

Because the cluster beam consists of a wide range of mixed clusters, a shutter at the exit of the oven is used to confirm the presence of magnesium in the signal by noting the difference in intensity when the shutter is open and closed. As there are three Mg isotopes ($^{24}Mg = 78.99$, $^{25}Mg = 10.00$, $^{26}Mg = 11.01$), comparison can be made between three different precursor ion intensity distributions. To minimize errors, many of the measurements presented here were repeated over a number of experimental sessions.

Neutral clusters, some of which contain (on average) a single metal atom enter the ion source of a high-resolution reverse geometry double focusing mass spectrometer (VG-ZAB-E), where they are ionized by high-energy electron impact (~70−100 eV). Because only ions rather than neutral complexes are detected in the experiment, it is likely that extensive evaporation of ligands, predominantly argon, but also ammonia molecules, takes place to reduce the internal energy of the complexes to a relatively stable level. Accordingly, under most experimental conditions no ion complexes of the form $[M(L)_n(Ar)_m]^{z+}$ have been detected, where M = metal species, L = ligand and *n* and *m* are integers.

Mass analyzed kinetic energy spectroscopy (MIKES)[24] has been employed extensively to analyze the stability and chemical reactivity of ions from the series $[Mg(NH_3)_n]^{2+}$. From such measurements, we can infer details of the structure and reactions pathways adopted by ions of a certain size. It is possible to study both the unimolecular (metastable) decay pathways as well as collision activated dissociation pathways occurring in the second field free region (2nd ffr) of the mass spectrometer. A collision cell is located in this region, and slits either side of the cell allow the ion beam to enter and exit, while keeping the escape of collision gas to a minimum. As will be seen, several different fragmentation pathways can be activated by collision with a neutral gas, and a number of gases have been used, including He, N_2, O_2, and Xe, to investigate not only the fragmentation routes but also the influence the physical properties of a collision gas may have on the pathway taken. Collision gas is introduced into the cell via a needle valve and sufficient gas is added to reduce the precursor ion intensity by ~50%. When comparisons are made between different collision gases, the measurements are made at a specific pressure (usually 10^{-6} mbar) and the data are then corrected for variations in detection efficiency of the gases at an ion gauge.

The vacuum in the flight tube as a whole does not change significantly, as differential pumping is located close to the cell. To provide accurate differentiation between processes taking place within the collision cell and those occurring elsewhere within the flight tube, a voltage can be applied to the cell. Under normal circumstances, the laboratory-frame kinetic energy of a fragment ion, E_f, can calculate from the expression

$$E_f = \frac{m_f q_p}{m_p q_f} E_p \qquad (1)$$

where m_f and m_p are the masses of the fragment and parent ions, respectively, and q_f and q_p are their charges. With the addition of a voltage, V_c, to the collision cell, a separate, collision-induced signal can be detected at a kinetic energy E_{fc}, which is given by the expression

$$E_{fc} = \frac{m_f q_p}{m_p q_f} + \frac{m_p q_f - m_f q_p}{m_p q_f} V_c \qquad (2)$$

The precise voltage applied to the cell was calibrated using the collision-induced reactions of CO_2^{2+}.

The MIKES technique[24] has also been used to study two types of unimolecular fragmentation under circumstances where there was no collision gas in the cell and the pressure in the flight tube remained below 10^{-7} mbar. In these experiments fragmentation relied on the presence of internal energy remaining after electron impact ionization and, as will be seen, this promoted two separate pathways: (i) charge separation in small complexes; (ii) neutral molecule loss in larger complexes.

Compared with many of our earlier experiments, the data from MIKE scans presented here have been recorded under conditions where there has been a significant improvement in energy resolution and sensitivity. As a result, it is now possible to distinguish unambiguously between fragmentation pathways that differ by ±1 amu. In the past, our inability to make this assignment has caused problems with interpretation.

Results

A. Ion Intensities. Figure 1 shows a precursor ion intensity distribution recorded for $[Mg(NH_3)_n]^{2+}$ ions, where distributions recorded at different times have been averaged. Intensities were measured by taking the difference between ion signals recorded with the shutter above the oven open and closed. However, it

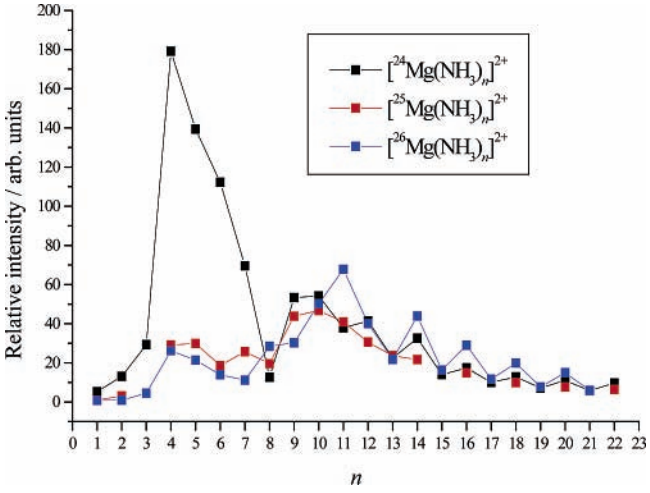

Figure 1. Relative ion intensities as a function of *n* recorded for the series $[Mg(NH_3)_n]^{2+}$. Data are presented for each of the three isotopes of magnesium.

is still not possible to rule out completely any interference from background nonmetallic signals that may also be part of the pulsed ion beam passing through the mass spectrometer. The most pronounced interference occurs at $m/z = 80$ between $[^{24}Mg(NH_3)_8]^{2+}$ and Ar_2^+, which is always present in the ion beam. However, there is also a source of interference, as yet unidentified, with the minor magnesium isotopes for $n > 7$, which causes their intensities to be greater than those derived from the isotope distribution.

Precursor ion intensity distributions, of the type shown in Figure 1, can be complex to interpret. The final step in the production of these solvated species is electron impact ionization at 70−100 eV with the result that ions emerging from the source have high internal energies. Under the nonequilibrium conditions present in these experiments, there is no opportunity for ions to "grow" by association; as a function of time, they can either fragment and/or undergo radiative decay to reduce their internal energy content and gain stability. Any distribution of multiply charged ions is thus weighted toward lower numbers as higher members of the series undergo neutral molecule loss as well as possible charge transfer. There is also a marked bias against very small multiply charged clusters as these are unstable with respect to charge transfer. Because ions with relatively high internal energies and/or relatively low binding energies will have high rates of decay relative to more stable ions, at the point of observation ($\sim 10^{-4}$s) certain ions will have evolved with greater intensity. In Figure 1, data for ^{24}Mg show a sharp increase between $n = 3$ and 4, followed by a stepwise decline from $n = 4$ to $n = 8$. Beyond $n = 8$, the ion intensities are low, but it is still possible to discern slight increases for $n = 9$ and $n = 10$ followed by a relatively slow decline where differences between adjacent complexes become difficult to quantify. The distribution recorded in these experiments is very similar to that given by Okai et al.[25] following the formation of $[Mg(NH_3)_n]^{2+}$ complexes via multiphoton ionization. Overall, the intensity data from the two experiments would suggest that $[^{24}Mg(NH_3)_4]^{2+}$ is particularly stable with respect to its nearest neighbors. Previous measurements of ion intensity distributions, which showed regions with a relatively slow decline in intensity have been interpreted in terms of the formation of a hydrogen-bonded network.[7,8] Earlier studies of $[Mg(NH_3)_n]^{2+}$ complexes concluded that $n = 3$ was the smallest stable species.[9] In these current experiments ions down to $n = 1$, $[MgNH_3]^{2+}$, have been observed.

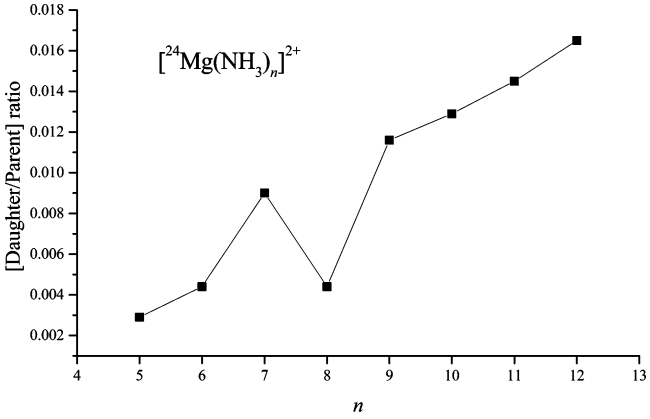

Figure 2. Plot of the Fragment/Precursor ion ratio as a function of *n* for the metastable unimolecular reaction $[^{24}Mg(NH_3)_n]^{2+} \rightarrow [^{24}Mg(NH_3)_{n-1}]^{2+} + NH_3$.

B. Unimolecular Fragmentation Patterns. Taken alone, ion intensity data do not always provide convincing evidence of ion stability. However, the relative stabilities of ions from a series, such as $[^{24}Mg(NH_3)_n]^{2+}$, can also be investigated using the MIKE technique to follow their fragmentation patterns. Ions emerging from the source with lifetimes in the range 10^{-5}−10^{-4} s can be expected to undergo metastable (unimolecular) decay in the region between magnetic and electric sectors (2nd ffr). Such measurements on fragmentation can help in understanding the structure of solvated species, as the rate constant for a specific decay process will be a function of cluster size and stability. An analysis of the kinetic conditions that underpin competition between fragmentation pathways in ions shows that metastable decay is dominated by the most facile fragmentation route (competitive shift), and this may change with increasing cluster size and/or composition.[26] Figure 2 shows the intensity ratio of the product and precursor ions recorded as a function of *n* for the metastable fragmentation pathway:

$$[Mg(NH_3)_n]^{2+} \rightarrow [Mg(NH_3)_{n-1}]^{2+} + NH_3 \qquad (3)$$

Attempts were made to measure this ratio for all $[^{24}Mg(NH_3)_n]^{2+}$ ions in the range 2−14; however, reaction 3 was only observed for $n \geq 5$. An alternative decay route for ions where $n < 5$ is discussed in more detail below. In general, the relative intensities of product ions from any series, such as in (3), should increase monotonically with *n*. This effect is due to several factors; first, larger ions will have more degrees of freedom over which energy can be randomized, which will both increase their lifetime with respect to decay and increase their heat capacity. Second, from a statistical standpoint, the loss of one ammonia molecule becomes more probable as *n* increases. Finally, heavier ions will move more slowly through the second field free region, and this will increase the time scale over which ions have to fragment. The graph shows that between $n = 6$ and $n = 7$ there is a relatively steep increase in intensity for the product ion, which indicates that $n = 7$ is susceptible to the loss of a single ammonia molecule, suggesting that the reaction barrier is small compared with other members of the series. The gradients between $n = 5$ and 6 and between $n = 9$ and 12 are all very similar, suggesting that there is no extra stability associated with these ions. As noted above, the result at $n = 8$ is probably influenced by interference from Ar_2^+.

In contrast to the results presented for larger clusters, the metastable fragmentation pathway observed for smaller clusters $[Mg(NH_3)_n]^{2+}$ ($n \leq 4$) is a proton transfer (charge separation) process:

$$[Mg(NH_3)_n]^{2+} \rightarrow [(NH_2)Mg(NH_3)_{n-2}]^+ + NH_4^+ \quad (4)$$

The MIKE technique has been used to record peak profiles for the metal-containing products of reaction 4 when $n = 3$ and 4, and these are shown in Figure 3. Because reaction 4 involves charge separation, the peak profiles that accompany the fragments are much broader than those seen from clusters that lose neutral fragments.[24] As with the neutral-loss processes discussed above, the peak profiles seen in Figure 3 are the products of metastable (unimolecular) decay; the effects of introducing a collision gas are discussed below. Although the ion signal for $[Mg(NH_3)_2]^{2+}$ was reasonably strong, no decay products of the type shown in Figure 3, were observed.

The increased width of the peaks seen in Figure 3 is because of high kinetic energy release (KER), which originates from Coulomb repulsion between the two separating point charges. Dish-shaped profiles, of the type shown are due to instrumental discrimination against fragment ions ejected perpendicular to the laboratory-frame flight direction. The edges of such peaks correspond to ions that have center-of-mass velocities that either add to or subtract from the laboratory-frame velocity vector. The high kinetic energy edge of each peak often has greater intensity compared with the low kinetic energy edge because the ions that contribute to the latter are moving more slowly and are, therefore, the subject of increased discrimination. The maximum center-of-mass kinetic energy with which the charged fragments can emerge is given by the potential energy difference between the two charged states (approximately second IE of the metal minus the first IE of the ligand), which in this case is 4.96 eV. Taking the fwhm (full-width at half-maximum) values of the peaks the center-of-mass kinetic energy release, T, can be calculated using the expression[24,27]

$$T = \frac{y^2 m_p{}^2 V}{16 x m_d (m_p - m_d)} \left(\frac{\Delta E}{E_o}\right) \quad (5)$$

where x is the charge on parent ion, y is the charge on fragment ion, m_d is the mass of the fragment ion, m_p is the mass of the parent ion, and V is the ion source accelerating voltage, ΔE is the fwhm value of the peak profile, and E_o is the laboratory-frame kinetic energy of the precursor ion. The values for T calculated from the widths of peaks (a) and (b) of Figure 3 are 2.14 and 1.88 eV, respectively. It is to be expected that the kinetic energy release measured for the smaller ion will be higher, because at the point of dissociation the point charges are closer together and thus the degree of Coulombic repulsion will be larger. It is also possible that the kinetic energy release measured for the larger complex is further reduced because of an increased number of degrees of freedom into which some fraction of the repulsive energy can be partitioned.[24] The most significant observation to emerge from these measurements on metastable (unimolecular) decay, is the dramatic switch in fragmentation pathway, from charge separation at $n = 4$ to the loss of neutral NH_3 at $n = 5$.

The intensity and fragmentation data recorded thus far would suggest that $[^{24}Mg(NH_3)_4]^{2+}$ is a critical configuration, in terms of either stability or structure. In a series of important papers Glusker and co-workers[28−32] have noted that, with reference to the Cambridge Structural Database (CSD) and calculations, magnesium prefers ligands that are oxygen donors rather than nitrogen donors and also has a preference for six ligands bound directly to the central metal ion. However, it is known that gas-phase studies have a propensity toward lower coordination numbers and also the lack of bulk solvation favors extended hydrogen-bonded networks.[33,34] Stace has concluded that ligands capable of forming strong hydrogen bonds, i.e., water, have a smaller number of ligands coordinated directly to the central ion than those forming weaker hydrogen bonds, i.e., ammonia.[35] Density functional calculations by Shoeib et al.[17] on singly charged species of $[Mg(NH_3)_n]^+$, for $n = 1-6$, coordinate all of the ammonia molecules directly to the metal; however, the free energies for $n = 5$ and 6 were found to be very small. At values of $n > 6$, the same calculations showed complexes where the seventh and eighth ammonia molecules were coordinated to the inner solvation shell via hydrogen bonding. It would be expected that coordination through a nitrogen atom, should result in a single hydrogen bond to a hydrogen atom on the inner shell. Instead, the calculations showed that these outer ammonia molecules were positioned between two inner molecules forming a "double" hydrogen bond, suggesting that the nitrogen atoms in the solvating molecules are five-coordinate. However, the free energies of formation of these (6+0), (6+1) and (6+2) structures were found to be zero, if not positive.[17] Similar, five-coordinate nitrogen atoms have been found following calculations on $[Cu(NH_3)_n]^{2+}$ complexes when $n > 4$.[36] In the case of dications, the formation of single and double hydrogen bonds is probably aided through the formation of *charge-enhanced bonds*, where the protic character of inner shell hydrogen atoms is increased through polarization of electron density by the positive charge.

From the data presented here it is not possible to conclude whether ligands are either coordinated directly to the metal ion or part of a hydrogen-bonded structure. Evidence of a dramatic switch in fragmentation pattern at $n > 4$ might suggest that the first four ammonia molecules are bound directly to the central magnesium dication. However, the fact that charge separation on the part these smaller complexes, involves the loss of NH_4^+, would imply that there is some movement of molecules from the inner to an outer solvation shell during the course of a reaction. The switch in behavior at $n = 5$ also suggests a significant change in environment, which possibly coincides with the increased occupation of a second/outer solvation shell, where conformers of the form (4+x) have enhanced stability compared with direct coordination to the metal ion. Earlier studies of $[Cu(H_2O)_n]^{2+}$ and $[Cu(NH_3)_n]^{2+}$ support this conclusion.[34,37]

C. Collisional-Induced Dissociation (CID) and Electron Capture. A significant contribution toward analyzing the stabilities of multiply charged metal−ligand complexes, has come from studies of their reactivity following collisional activation.[1,13,14,38] These studies have identified three main fragmentation patterns: (i) neutral loss of a ligand molecule; (ii) charge reduction (electron or proton transfer); (iii) heterolytic bond cleavage within individual ligand molecules, as reported by Shvartsburg and co-workers.[6,39] This latter behavior contrasts markedly with metastable (unimolecular) studies, where the only evidence of reactivity is in the form of proton transfer that accompanies Coulomb explosion (reaction (4) above). The activation of a precursor ion with collision gas can be seen as a two-step process. First, there is the transfer of energy from the collision gas to the precursor ion, and although it was originally thought that low energy collisions involved only vibrational excitation and high-energy collisions exclusively electronic excitation, it is now believed that a number of "limiting-case" mechanisms underlie CID and that they are not easily differentiated.[40,41] For a closed-shell species, such as $[Mg(NH_3)_n]^{2+}$,

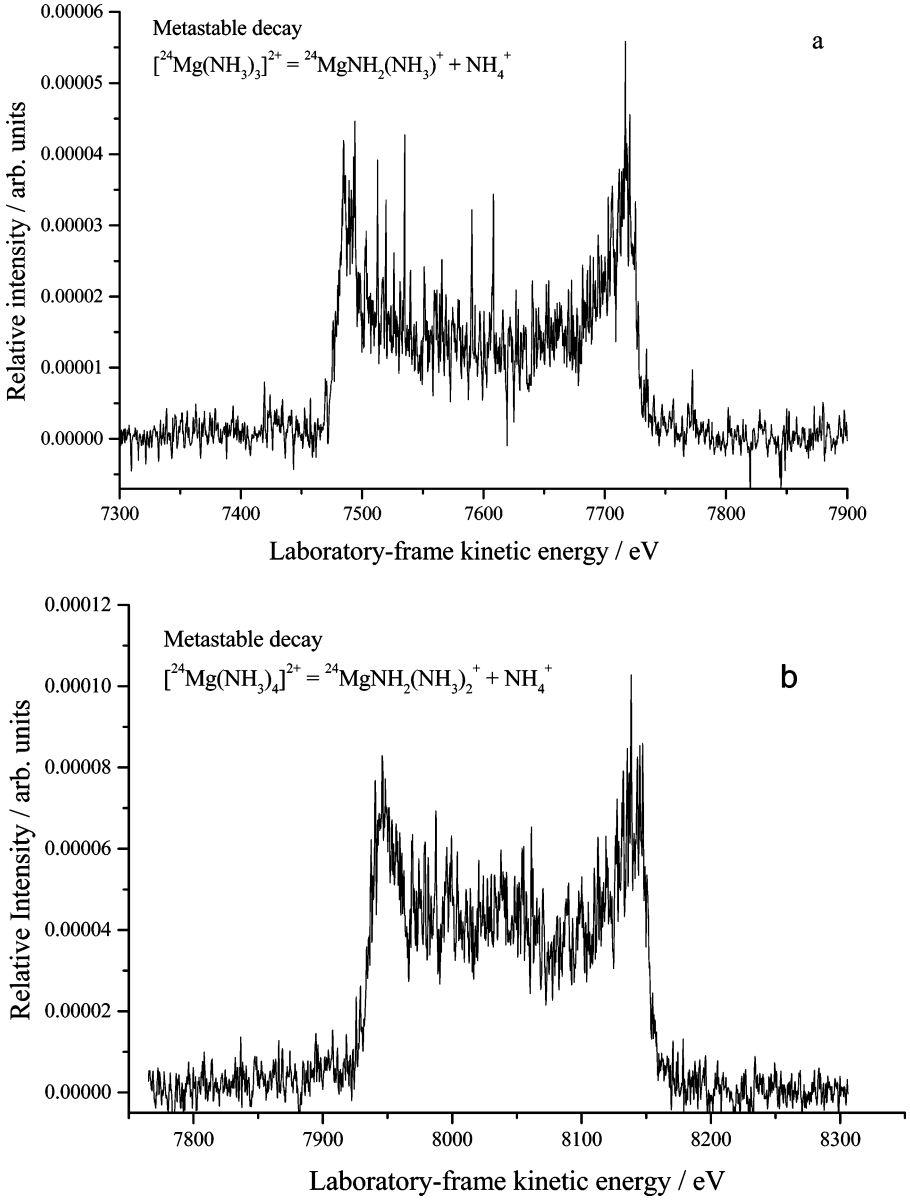

Figure 3. Kinetic energy profiles recorded following the metastable unimolecular fragmentation of (a) $[Mg(NH_3)_3]^{2+}$ to produce $[(NH_2)Mg(NH_3)]^+ + NH_4^+$ and (b) $[Mg(NH_3)_4]^{2+}$ to produce $[(NH_2)Mg(NH_3)_2]^+ + NH_4^+$. In both cases, the peak shapes are indicative of Coulomb explosion.

electronic excitation is energetically unfavorable and, therefore collisional activation probably involves vibrational degrees of freedom. The second step of the CID process is dissociation, where the degree of fragmentation will depend on the total internal energy of the excited precursor ion.[41]

From a consideration of the charge reduction pathways seen in the metastable studies discussed above, charge transfer might also be expected following collisional activation and could be identified as collision-induced charge separation dissociation (CICSD) as described by reaction 6. The magnitude of any

$$[M(L)_n]^{2+} + CG \rightarrow [M(L)_n]^{2+*} \rightarrow [M(L)_{n-k-1}]^+ + L^+ + kL \quad (6)$$

kinetic energy release as well as the overall peak shape are likely to differ slightly from those found under metastable (collision-free) conditions. Because collisional activation could lead to a significantly different internal energy distribution, it is very likely that the range of kinetic energies with which the product ions emerge will also differ from that seen following metastable decay. The most obvious outcome is a "filling-in" of the characteristic dish-shaped profile (cf Figure 3). Unlike metastable decay, CID processes do not have to involve internal ion energies that precisely match a decay time window; hence there is a far greater spread in kinetic energies, with the result that there is always some fraction of ions where the energy release is small enough not to experience instrumental discrimination.

In the case of multiply charged metal−ligand complexes; collisions with a background gas can also offer alternative charge reduction mechanisms. Dissociation pathways involving the production of singly charged species have frequently been assumed to be caused either by internal electron transfer from a ligand to the metal or possibly by proton transfer when associated with protic ligands, such as ammonia or water. However, charge separation is not the only charge-reduction route available in the presence of a collision gas. Charge-exchange in the form of "electron capture" from the collision gas is also common,[24] and in the case of a dication, the resultant singly charged ion can acquire sufficient internal energy for fragmentation, leading to electron capture-induced

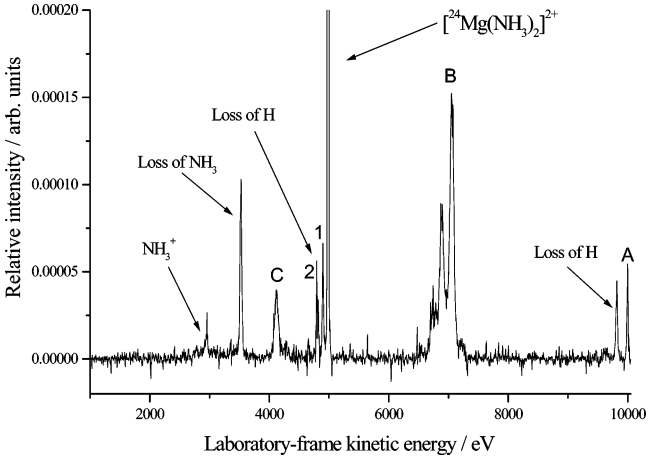

Figure 4. MIKE spectrum of $[Mg(NH_3)_2]^{2+}$ following collisional activation with O_2 at a pressure of $\sim 10^{-6}$ mbar in the collision cell. The origins of the features labeled A−C are discussed in the text.

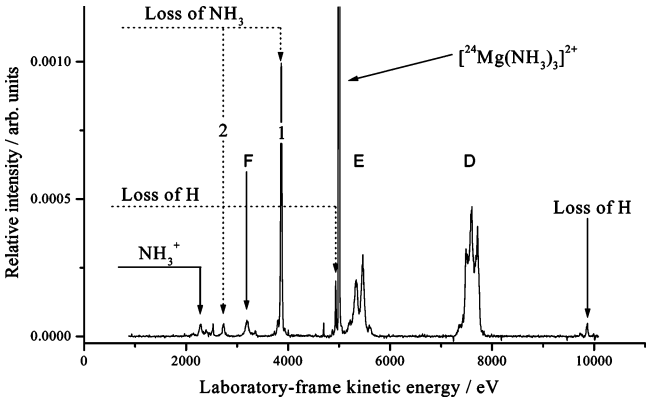

Figure 5. As for Figure 4, but $[Mg(NH_3)_3]^{2+}$. The origins of the features labeled D−F are discussed in the text.

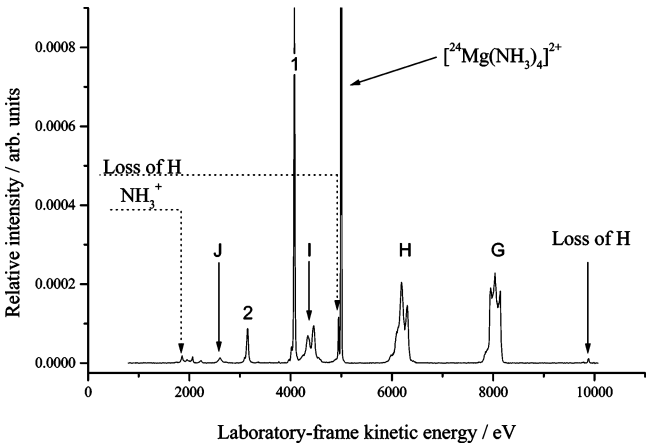

Figure 6. As for Figure 4, but $[Mg(NH_3)_4]^{2+}$. The origins of the features labeled G−J are discussed in the text.

dissociation (ECD) in the form

$$[M(L)_n]^{2+} + CG \rightarrow [M(L)_n]^{+} + CG^{+} \rightarrow [M(L)_{n-k}]^{+} + kL \quad (7)$$

Figures 4−6 show examples of MIKE scans recorded following the collisional activation of $[Mg(NH_3)_2]^{2+}$, $[Mg(NH_3)_3]^{2+}$ and $[Mg(NH_3)_4]^{2+}$ with O_2 as a collision gas (unless otherwise stated, all MIKE scans involved the most abundant isotope ^{24}Mg). As far as the loss of neutral species is concerned, the scans have several features in common, including the

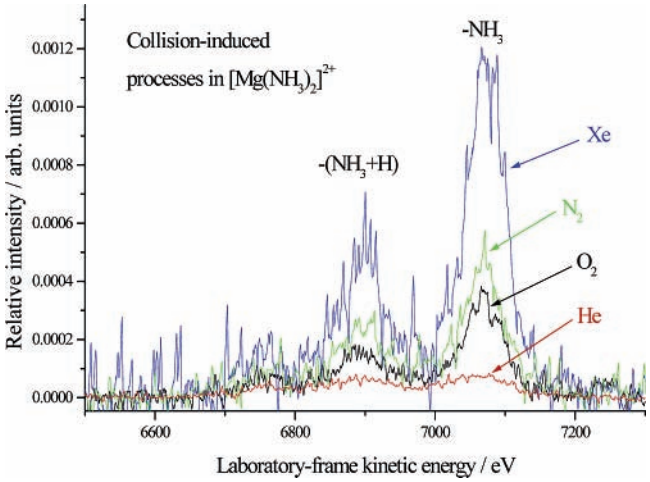

Figure 7. Kinetic energy profiles of ionic fragments from $[Mg(NH_3)_2]^{2+}$ recorded following collisional activation with the gases He, Xe, N_2, and O_2 at a pressure of $\sim 10^{-6}$ mbar in the collision cell. The complementary neutral fragments are identified at each peak.

multiple loss of both ammonia molecules (eq 8) and hydrogen atoms (eq 9) from the precursor ion.

$$[Mg(NH_3)_n]^{2+} \rightarrow [Mg(NH_3)_{n-k}]^{2+} + kNH_3 \quad (8)$$

$$[Mg(NH_3)_n]^{2+} \rightarrow [(NH_{3-k})Mg(NH_3)_{n-1}]^{2+} + kH \quad (9)$$

On close inspection, Figures 4−6 also show a number of features associated with charge reduction processes, which in previous studies of metal−ammonia dication complexes have been identified as NH_3^+ or NH_4^+ loss caused by charge transfer from a ligand to the metal.[42,43] However, when compared with Figure 3, it is quite clear that many of the features do not display the large kinetic energy spread associated with charge separation.

In the case of $[Mg(NH_3)_2]^{2+}$ (Figure 4) the presence of a peak at 10 000 eV (labeled as A) suggests that electron capture occurs to form $[Mg(NH_3)_2]^{+}$ without dissociation. In some instances, peaks observed at 10 000 eV were found not to be metal dependent; however, checks undertaken at a reduced oven temperature were able to confirm that, for small values of n, these peaks were due to electron capture on the part of $[Mg(NH_3)_n]^{+}$ complexes. All three multiply charged ions ($n = 2-4$) provide evidence of electron capture followed by H atom loss in the form of the reaction

$$[Mg(NH_3)_n]^{2+} + CG \rightarrow [Mg(NH_3)_n]^{+} + CG^{+} \rightarrow [NH_2Mg(NH_3)_{n-1}]^{+} + H \quad (10)$$

Obviously, the charge-transfer equivalent for this reaction, which would lead to the appearance of H^+, is also possible and could account for the peak seen in each of the scans. However, the high ionization energy of H would suggest that this pathway is unfavourable relative to either the more facile electron capture route or other alternative charge transfer pathways (e.g., reaction 4). As stated previously, reactions involving the loss of H have been observed from singly charged magnesium/molecule complexes.[7,18] In addition, earlier studies have shown that multiply charged complexes containing protic solvents can also lose varying numbers of H atoms without charge reduction.[43]

In view of the range of processes appearing to contribute to peak B in Figure 4, separate, high-resolution scans have been undertaken using several different collision gases and these results are shown in Figure 7. The only feature that might be

attributable to Coulomb explosion is the low-energy edge of a very weak dish-shaped peak at ~6750 eV (most prominent in the xenon data), and this corresponds to the step

$$[Mg(NH_3)_2]^{2+} \rightarrow Mg^+NH_2 + NH_4^+ \quad (11)$$

From the width at the base of the peak the accompanying kinetic energy release is approximately 4 eV, which represents a significant fraction of the maximum energy available (4.96 eV). The central narrow feature at ~6900 eV is attribute to ECD, and although it is not possible to specify whether neutral loss corresponds to either NH_4 or $NH_3 + H$, the overall reaction is

$$[Mg(NH_3)_2]^{2+} + CG \rightarrow [Mg(NH_3)_2]^+ + CG^+ \rightarrow Mg(NH_2)^+ + NH_3 + H \quad (12)$$

Finally, the most prominent feature, seen at ~7075 eV, corresponds to the loss of neutral NH_3, which again can be attributed to electron capture followed by fragmentation.

$$[Mg(NH_3)_2]^{2+} + CG \rightarrow [Mg(NH_3)_2]^+ + CG^+ \rightarrow Mg(NH_3)^+ + NH_3 \quad (13)$$

Peak C in Figure 4 is too narrow to be associated with charge separation and so is probably due to electron capture; its position corresponding to the process

$$[Mg(NH_3)_2]^{2+} + CG \rightarrow [Mg(NH_3)_2]^+ + CG^+ \rightarrow Mg^+ + 2NH_3 \quad (14)$$

Finally, in Figure 4, there is a peak at 2958 eV, which corresponds to the appearance of NH_3^+. This product is interesting because it does not equate with any of the reactions identified above. Direct charge-transfer always leads to the appearance of NH_4^+ and the equivalent process to give NH_3^+ might have been expected to be accompanied by a much broader peak than is seen at 2958 eV. One possibility is for electron capture to be accompanied by charge transfer, i.e.

$$[Mg(NH_3)_2]^{2+} + CG \rightarrow [Mg(NH_3)_2]^+ + CG^+ \rightarrow (Mg + NH_3) + NH_3^+ \quad (15)$$

An analogous pathway suggested by calculations on the low-lying excited states[19] involves vertical excitation ($\Delta E = 4.01$ eV) from the ground state of $[Mg(NH_3)_2]^+$. Unlike $[Mg(NH_3)_3]^{2+}$ and $[Mg(NH_3)_4]^{2+}$, where metastable charge separation is observed (see Figure 3), the processes identified above for $[Mg(NH_3)_2]^{2+}$ are all collision-induced. The loss of neutral NH_3 by the ion confirms the observation of $[MgNH_3]^{2+}$ as a stable ion.

Having identified a variety of reaction pathways associated with $[Mg(NH_3)_2]^{2+}$, we are now in a position to see how these develop as the size of the complex is increased. Figures 5 and 6 show results from MIKE scans on $[Mg(NH_3)_3]^{2+}$ and $[Mg(NH_3)_4]^{2+}$ following collisional activation with O_2. One feature they have in common is the loss of hydrogen atoms both from the precursor ions and from charge reduced products. Both processes are observed to decline in significance as the complexes increase in size and are absent for $n \geq 5$.

From their positions in Figure 5, peaks D and E can be identified as charge reduced products originating from $[Mg(NH_3)_3]^{2+}$. Figure 3a shows reaction 3 occurring as a unimolecular process, and Figure 8 shows an expanded view of the same energy region, but with N_2 as a collision gas and a voltage of 963 V applied to the collision cell. As predicted earlier, the dished profile due to the unimolecular charge separation processes (Figure 3b) has fill-in as a result of gas leakage from the cell. Features attributed to processes taking place within the cell have shifted to a new laboratory frame kinetic energy, E_{fc}, as given by eq 2. Peak D of Figure 5 now appears as a composite of three processes: (i) Coulomb explosion and charge separation:

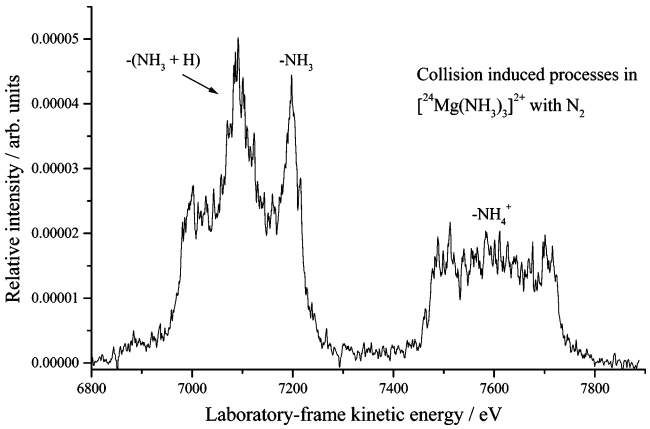

Figure 8. Kinetic energy profiles of ionic fragments from $[Mg(NH_3)_3]^{2+}$ recorded following collisional activation with N_2 at a pressure of $\sim 10^{-6}$ mbar in the collision cell, which was floated at a voltage of 963 V. The complementary neutral and ionic fragments are identified at each peak.

$$[Mg(NH_3)_3]^{2+} \rightarrow [NH_2MgNH_3]^+ + NH_4^+ \quad (16)$$

with a kinetic energy release of 2.46 eV; (ii) a central narrow feature at ~7100 eV corresponding to the ECD process:

$$[Mg(NH_3)_3]^{2+} + CG \rightarrow [Mg(NH_3)_3]^+ + CG^+ \rightarrow [NH_2MgNH_3]^+ + NH_3 + H \quad (17)$$

and a further narrow peak at ~7200 eV corresponding to a second ECD step:

$$[Mg(NH_3)_3]^{2+} + CG \rightarrow [Mg(NH_3)_3]^+ + CG^+ \rightarrow [Mg(NH_3)_2]^+ + NH_3 \quad (18)$$

Note the changes in the relative intensities of the products from the above reactions (peak D in Figure 5) when compared with similar data from $[Mg(NH_3)_2]^{2+}$ (peak B in Figure 4). This aspect of the results will be the subject of further discussion below.

For E in Figure 5 the separate peaks are attributed to the reactions:

$$[Mg(NH_3)_3]^{2+} + CG \rightarrow [Mg(NH_3)_3]^+ + CG^+ \rightarrow [NH_2Mg]^+ + 2NH_3 + H \quad (19)$$

and

$$[Mg(NH_3)_3]^{2+} + CG \rightarrow [Mg(NH_3)_3]^+ + CG^+ \rightarrow [MgNH_3]^+ + 2NH_3 \quad (20)$$

Finally, peak F corresponds to the following electron capture reaction:

$$[Mg(NH_3)_3]^{2+} + CG \rightarrow [Mg(NH_3)_3]^{+} + CG^{+} \rightarrow Mg^{+} + 3NH_3 \quad (21)$$

A peak can also be identified at 2292 eV corresponding to the appearance of NH_3^+. As noted earlier, the peak is too narrow for charge separation but may originate from a combination of electron capture and charge transfer (i.e., similar to reaction 14).

For $[Mg(NH_3)_4]^{2+}$ it is possible to identify from the MIKE scan reactions that are analogous to those discussed above, but involving one additional NH_3 molecule. For the purposes of a detailed comparison, one feature of the scan (peak G) has been examined with a range of collision gases and with a voltage of 963 V applied to the collision cell. These results are shown in Figure 9 where it can be seen that the feature again separates into two components, one associated with unimolecular charge separation (~8000 eV) and the other a combination of the latter together with ECD processes. The ECD reactions, which are clearly separated with O_2 as a collision gas, correspond to the loss of $NH_3 + H$ (~7450 eV) and NH_3 (~7520 eV). Note again the change in the relative intensities of these two processes compared with earlier examples seen for $[Mg(NH_3)_2]^{2+}$ and $[Mg(NH_3)_3]^{2+}$. Returning to Figure 6, peaks H and I are similar ECD reactions to those identified above but involve additional NH_3 molecules. Finally, peak J corresponds to the appearance of Mg^+ and there is also a peak at ~1856 eV, which is due to the appearance of NH_3^+.

As a final example of how electron capture contributes to the decay pattern of multiply charged metal−cation complexes, Figure 10 shows the result of a MIKE scan recorded for $[Mg(NH_3)_8]^{2+}$ in the presence of O_2 as a collision gas. As can be seen, the charge reduction region above 5000 eV is dominated by a sequence of narrow peaks, the majority of which correspond to the loss of $k$$NH_3$ molecules, where $k = 1-4$; however, there is also evidence of NH_3 loss being accompanied by the additional loss of an H atom. There are two further aspects to the scan that are of interest, first, the underlying width of the ECD peaks increases following the loss of five and six NH_3 molecules. The onset of such behavior coincides with the processes that contribute to the composite peak resulting from the break up of $[Mg(NH_3)_4]^{2+}$, as seen in Figures 6 (peak G) and 9. The second point of interest may be related to the latter, and this is the observation that $[Mg(NH_3)_8]^{2+}$ readily loses four neutral NH_3 molecules (the appropriate peaks are labeled in Figure 10); however, thereafter, the intensities of neutral loss peaks are minimal. MIKE scans of $[Mg(NH_3)_7]^{2+}$, $[Mg(NH_3)_6]^{2+}$ and $[Mg(NH_3)_5]^{2+}$ (not shown) exhibit comparatively intense peaks due to the loss of three, two and one NH_3, respectively, prior to a marked reduction in the intensities of such signals. If each of these ions decays down to $[Mg(NH_3)_4]^{2+}$ and then undergoes Coulomb explosion, this would account for the increase in width noted above and the near absence of any neutral loss peaks from fragments below $[Mg(NH_3)_4]^{2+}$. Although ECD would appear to be the dominant charge reduction process for $[Mg(NH_3)_8]^{2+}$, as a percentage of the total fragment ion intensity, it amounts to <5%, with neutral loss being the most significant reaction pathway.

It was noted earlier that there appears to be a competition between loss of NH_3 and loss of $NH_3 + H$ following ECD, and to summarize the appropriate data, Figure 11 shows the percentage of each of these fragments originating from size-selected complexes. As seen from Figure 10 and confirmed here for $n = 6$ and 7, the dominant ECD route for larger complexes is the loss of one or more neutral NH_3 molecules. However, at the critical fragment size of $n = 4$, the loss of neutral NH_3 accompanied by the loss of a hydrogen atom becomes the dominant fragmentation pathway. Finally, at the point where fragmentation leads to either $MgNH_2^+$ or $MgNH_3^+$, the latter (corresponding only to the loss of whole molecules) once again becomes the more intense fragment. Confirmation of the latter is seen in Figures 5 (peak E) and 6 (peak I).

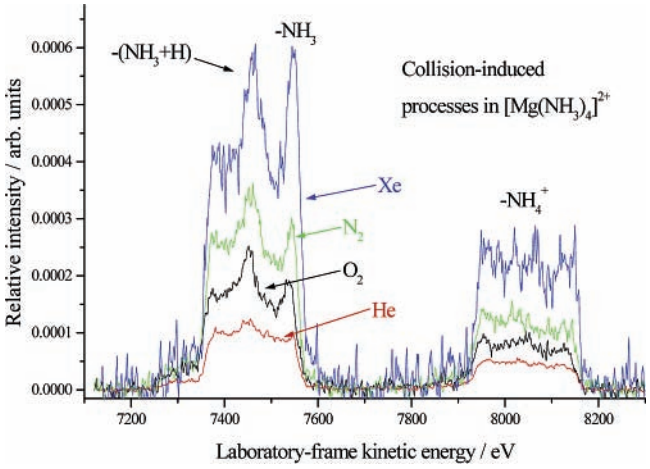

Figure 9. Kinetic energy profiles of ionic fragments from $[Mg(NH_3)_3]^{2+}$ recorded following collisional activation with the gases He, Xe, N_2, and O_2 at a pressure of $\sim 10^{-6}$ mbar in the collision cell, which was floated at a voltage of 963 V. The complementary neutral and ionic fragments are identified at each peak.

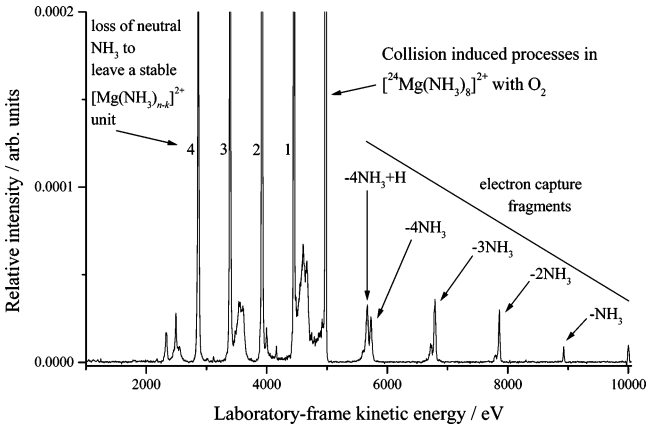

Figure 10. MIKE spectrum of $[Mg(NH_3)_8]^{2+}$ following collisional activation with O_2 at a pressure of $\sim 10^{-6}$ mbar in the collision cell.

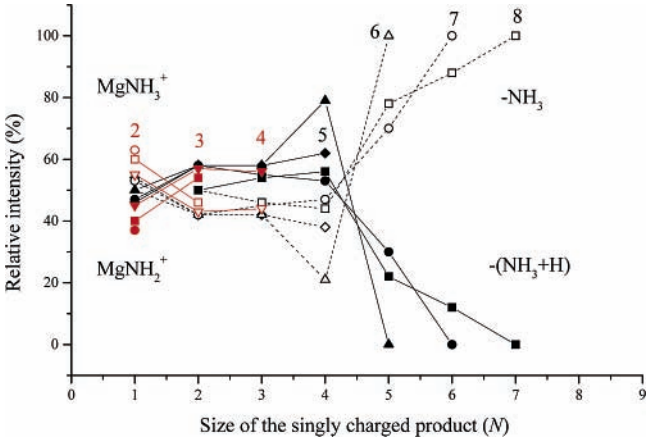

Figure 11. Preferential neutral loss channels following electron capture. The individual ions selected for study are identified within the figure. The open symbols correspond to loss of neutral NH_3 and the closed symbols to the combined loss of neutral $NH_3 + H$. For the purposes of identifying the size of the neutral product (N), the NH_2 fragment is counted as a molecule.

Discussion

From the results presented above, it is clear that the fragmentation pattern of $[Mg(NH_3)_n]^{2+}$ complexes involves three principal pathways: (i) metastable charge separation to give NH_4^+; (ii) metastable loss of neutral NH_3 molecules; (iii) electron capture induced dissociation to give NH_3 and (NH_3 + H), together with steps involving multiplies of NH_3. There are also collision-induced contributions to (i) and (ii), together with minor pathways, such as the loss of hydrogen. (i) and (ii) exhibit a distinct size effect; (i) is not seen in $[Mg(NH_3)_2]^{2+}$ and then stops abruptly after $[Mg(NH_3)_4]^{2+}$ to be replaced by (ii). In contrast, (iii) exhibits a gradual transition where the loss of NH_3 dominates the larger complexes, but the loss of (NH_3 + H) gains in intensity as their size decreases. At a qualitative level, it is possible to equate several of these pathways with the adoption of a particular molecular configuration. For $[Mg(NH_3)_n]^{2+}$ ions with $n = 3$ and 4 to lose NH_4^+ it is probably necessary for one molecule to be promoted into the second solvation shell, from where it can abstract a proton from a molecule in the primary shell. Such a process will be aided through the formation of charged enhanced hydrogen bonds of the type identified from other studies of multiply charged complexes,[35] and a suitable sequence of events has previously been calculated for $[Pb(H_2O)_n]^{2+}$ and $[Sn(H_2O)_n]^{2+}$ complexes.[44] It is also quite possible that some of the complexes appear as (2+1) and (3+1) units in the experiment as a consequence of electron impact. Likewise, for the loss of NH_3 to be the dominant ECD process in $[Mg(NH_3)_n]^{2+}$ for $n > 5$, would again suggest the presence of molecule(s) in an outer solvation shell, with the gradual switch to NH_3 + H loss coming once primary shell molecules are involved. Finally, what the latter step and the charge separation process have in common at $n \leq 4$ is they both lead to the appearance of $Mg^+NH_2(NH_3)_{n-2}$, which from Figure 11 is seen to be a favorable product. This observation somewhat contradicts the calculations of Daigoku and Hashimoto[45] who show $Mg^+NH_2(NH_3)_{n-1}$ + H to be much higher in energy than $Mg^+(NH_3)_n$, and the trend in their data would suggest that, as n increases beyond 4, the reaction leading to $Mg^+NH_2(NH_3)_{n-1}$ + H should become more favorable. However, the ECD and/or charge separation route to the formation of $Mg^+NH_2(NH_3)_{n-1}$ may not be the same as depicted in their calculations.

It is very evident from the results presented here at high collision energies that electron capture (ECD) rather than charge separation (charge transfer) is the dominant charge reduction process in the presence of a collision gas. Although electron capture has been seen in earlier experiments of this nature,[5,46,47] the events have not been correlated with either the appearance of specific ionic fragments or their kinetic energies. The advantage presented by the current study is that it has been possible to show that a number of distinct reaction channels arise as a direct result of electron capture and that, in each case, the fragment ion has associated with it a narrower distribution of kinetic energies than would be expected from Coulomb explosion. In several instances, identical metal-containing fragments are observed from electron capture and metal−ligand change transfer, but the latter are always accompanied by a more substantial release of kinetic energy.

Electron capture should be most efficient when the ionization energy of the collision gas is comparable to the electron affinity of the M^{2+} cation,[48] and capture cross-sections can be at least an order of magnitude larger than those estimated for collisional activation.[49] Figures 7 and 9 both include electron capture data recorded using a number of different collision gases. Two features of the results are apparent: first, xenon is the most efficient and helium the least efficient of the gases, and second, the nature of the gas has a marked influence on the relative intensities of the fragments. Again, this difference is most pronounced when helium is compared with xenon. Indeed, it is questionable whether helium promotes electron capture at all given the contribution that may come from residual air in the apparatus (see below).

An approximate calculation of the collision cross-section for electron capture can be obtained from a knowledge of the curve crossing point, r_c, for the two charged states, and an estimate of the crossing probability. The two curves can be represented by an ion-induced dipole interaction between the doubly charged metal complex and the collision gas, crossed at a point, r_c, by a repulsive Coulomb interaction between the singly charged products of electron transfer. The curve crossing point is easily estimated using expressions given previously[9] and, depending on the ionization energy of the collision gases, could be in the region 10−15 Å. The probability of crossing, p, can be estimated from the Landau−Zener equation,[49] $p = \exp(-2\pi H_{12}^2/\Delta F v_r)$, where H_{12} is one-half the adiabatic splitting at r_c, ΔF is the difference in slopes of the diabatic potential energy curves at r_c, and v_r is the relative velocity of the collision pair. The approximate cross-section is then given by $2\pi r_c^2 p(1-p)$. For the conditions that prevail in our particular experiment, estimates of the capture cross section are on the order of 10^{-15} cm^2,[49,50] which is to be compared with a hard-sphere CID cross section that could be at least an order of magnitude smaller. Given the similarities in their ionization energies, the difference between O_2 and xenon is somewhat surprising. However, the principal contribution to the calculation of both r_c and ΔF will be an ion-induced dipole interaction between the collision gas and $[Mg(NH_3)_n]^{z+}$, the strength of which will vary as αz^2, where α is the polarizability of the collision gas and z is the charge on the ion. Given that for xenon $\alpha = 4.1$ Å^3 and for O_2 $\alpha = 1.6$ Å^3, differences in the detail of their behavior might be expected. A comparatively large electron capture cross-section would account for the residual ECD contribution seen at the center of the profile shown in Figure 3b, which was at the lowest background pressure attainable in our experiments ($<10^{-7}$ mbar). Similar experiments on $[Mg(H_2O)_n]^{2+}$ complexes suggest that their ECD cross-sections are even larger than those suggested here for $[Mg(NH_3)_n]^{2+}$.[51]

In comparison to similar experiments undertaken on quadrupole mass spectrometers,[2−6] the results presented here have been obtained at much higher relative collision energies. Detailed calculations[50] on atomic systems show that the capture cross-section declines slightly as the collision energy is reduced; however, the results presented here would suggest that electron capture may play a greater role in determining the appearance of ionic fragmentations from $[ML_n]^{2+}$ complexes than has previously been appreciated.

Conclusions

The series $[Mg(NH_3)_n]^{2+}$ has been studied in terms of both the distribution of ions and their fragmentation patterns. It has been shown that for small n, metastable decay involves charge separation and, because of repulsion between two point charges at the instance of fragmentation, the release of a substantial amount of kinetic energy. For larger values of n, neutral loss of ammonia is the dominant metastable loss channel. The collisional activation of $[Mg(NH_3)_n]^{2+}$ ions yields fragment ion peak shapes that are indicative of electron capture, and it is concluded that electron capture dissociation (ECD) is the dominant charge reduction decay mechanism in the larger

($n > 4$) complexes. The onset of charge-transfer processes for when $n \leq 4$, may prevent collision-based techniques from being used to determine the binding energies of single molecules to metal dications.

Acknowledgment. We thank EPSRC for financial support for this program of experiments, and B.W. acknowledges the award of a Madame Chen Zhili scholarship and thanks Nottingham University for financial support.

References and Notes

(1) Stace, A. J. *J. Phys. Chem. A* **2002**, *106*, 7993.
(2) Blades, A. T.; Jayaweera, P.; Ikonomou, M. G.; Kebarle, P. *J. Chem. Phys.* **1990**, *92*, 5900.
(3) Blades, A. T.; Jayaweera, P.; Ikonomou, M. G.; Kebarle, P. *Int. J. Mass Spectrom., Ion Processes* **1990**, *101*, 325.
(4) Kohler, M.; Leary, J. A. *J. Am. Soc. Mass Spectrom.* **1997**, *8*, 1124.
(5) Kohler, M.; Leary, J. A. *Int. J. Mass Spectrom., Ion Processes* **1997**, *162*, 17.
(6) Shvartsburg, A. A.; Wilkes, J. G.; Lay, J. O.; Siu, K. W. M. *Chem. Phys. Lett.* **2001**, *350*, 216.
(7) Woodward, C. A.; Dobson, M. P.; Stace, A. J. *J. Phys. Chem. A* **1997**, *101*, 2279.
(8) Barran, P. E.; Walker, N. R.; Stace, A. J. *J. Chem. Phys.* **2000**, *112*, 6173.
(9) Walker, N. R.; Dobson, M. P.; Wright, R. R.; Barran, P. E.; Murrell, J. N.; Stace, A. J. *J. Am. Chem. Soc.* **2000**, *122*, 11138.
(10) Wright, R. R.; Walker, N. R.; Firth, S.; Stace, A. J. *J. Phys. Chem. A* **2001**, *105*, 54.
(11) Tonkyn, R.; Weisshaar, J. C. *J. Am. Chem. Soc.* **1986**, *108*, 7128.
(12) Weisshaar, J. C. *Acc. Chem. Res.* **1993**, *26*, 213.
(13) Märk, T. D. *Int. J. Mass Spectrom., Ion Processes* **1987**, *79*, 1.
(14) Schröder, D.; Schwarz, H. *J. Phys. Chem. A* **1999**, *103*, 7385.
(15) Andersen, A.; Muntean, F.; Walter, D.; Rue, C.; Armentrout, P. B. *J. Phys. Chem. A* **2000**, *104*, 692.
(16) Milburn, R. K.; Baranov, V. I.; Hopkinson, A. C.; Bohme, D. K. *J. Phys. Chem. A* **1998**, *102*, 9803.
(17) Shoeib, T.; Milburn, R. K.; Koyanagi, G. K.; Lavrov, V. V.; Bohme, D. K.; Siu, K. W. M.; Hopkinson, A. C. *Int. J. Mass Spectrom.* **2000**, *201*, 87.
(18) Yoshida, S.; Okai, N.; Fuke, K. *Chem. Phys. Lett.* **2001**, *347*, 93.
(19) Yoshida, S.; Daigoku, K.; Okai, N.; Takahata, A.; Sabu, A.; Hashimoto, K.; Fuke, K. *J. Chem. Phys.* **2002**, *117*, 8657.
(20) Misaizu, F.; Sanekata, M.; Fuke, K.; Iwata, S. *J. Chem. Phys.* **1994**, *100*, 1161.
(21) Berg C. B. M.; Achatz, U.; Joos, S.; Niedner-Schatteburg, G.; Bondybey, V. E. *Chem. Phys.* **1998**, *239*, 379.
(22) Walker, N. R.; Wright, R. R.; Stace, A. J. *J. Am. Chem. Soc.* **1999**, *121*, 4837.
(23) Del Mistro, G.; Stace, A. J. *Chem. Phys. Lett.* **1992**, *196*, 67.
(24) Cooks, R. G.; Beynon, J. H.; Caprioli, R. M.; Lester, G. R. *Metastable Ions*, 1st ed.; Elsevier: Amsterdam, 1973.
(25) Okai, N.; Yoshida, S.; Aranishi, K.; Takahata, A.; Fuke, K. *Phys. Chem. Chem. Phys.* **2005**, *7*, 921.
(26) Stace, A. J.; Shukla, A. K. *J. Am. Chem. Soc.* **1982**, *104*, 5314.
(27) Beynon, J. H.; Capriolo, R. M.; Richardson, J. W. *J. Am. Chem. Soc.* **1971**, *93*, 1852.
(28) Bock, C. W.; Kaufman, A.; Glusker, J. P. *Inorg. Chem.* **1994**, *33*, 419.
(29) Bock, C. W.; Kaufman Katz, A.; Glusker, J. P. *J. Am. Chem. Soc.* **1995**, *117*, 3754.
(30) Markham, G. D.; Glusker, J. P.; Bock, C. L.; Trachtman, M.; Bock, C. W. *J. Phys. Chem.* **1996**, *100*, 3488.
(31) Bock, C. W.; Katz, A. K.; Markham, G. D.; Glusker, J. P. *J. Am. Chem. Soc.* **1999**, *121*, 7360.
(32) George, P.; Glusker, J. P.; Markham, G. D.; Trachtman, M.; Bock, C. W. *Mol. Phys.* **2003**, *101*, 2451.
(33) Patwari, G. N.; Lisy, J. M. *J. Chem. Phys.* **2003**, *118*, 8555.
(34) Stace, A. J.; Walker, N. R.; Firth, S. *J. Am. Chem. Soc.* **1997**, *119*, 10239.
(35) Stace, A. J. *Phys. Chem. Chem. Phys.* **2001**, *3*, 1935.
(36) Berces, A.; Nukada, T.; Margl, P.; Ziegler, T. *J. Phys. Chem. A* **1999**, *103*, 9693.
(37) Walker, N. R.; Firth, S.; Stace, A. J. *Chem. Phys. Lett.* **1998**, *292*, 125.
(38) Schröder, D. *Angew. Chem., Int. Ed.* **2004**, *43*, 1329.
(39) Shvartsburg, A. A. *Chem. Phys. Lett.* **2002**, *360*, 479.
(40) Cooks, R. G. *J. Mass Spectrom.* **1995**, *30*, 1215.
(41) Shukla, A. K.; Futrell, J. H. *J. Mass Spectrom.* **2000**, *35*, 1069.
(42) Walker, N. R. Gas-Phase Studies of Multiply-Charged Transition Metal Complexes. Ph.D. Thesis, The University of Sussex, 1999.
(43) Duncombe, B. J.; Puskar, L.; Stace, A. J. Unpublished results.
(44) Cox, H.; Stace, A. J. *J. Am. Chem. Soc.* **2004**, *126*, 3939.
(45) Daigoku, K.; Hashimoto, K. *J. Chem. Phys.* **2004**, *121*, 3569.
(46) Seto, C.; Stone, J. A. *Int. J. Mass Spectrom., Ion Processes* **1998**, *175*, 263.
(47) Nielsen, A. B.; Hvelplund, P.; Nielsen, S. B. *Int. J. Mass Spectrom.* **2004**, *232*, 79.
(48) Hvelpund, P.; Anderseon, L. H.; Brink, C., Yu, D. H.; Lorents, D. C.; Ruoff, R. *Z. Phys. D* **1994**, *30*, 323.
(49) Olsen, R. E.; Salpo, A. *Phys. Rev. A* **1976**, *14*, 579.
(50) Ishii, K.; Itoh, A.; Okuno, K. *Phys. Rev. A* **2004**, *70*, 042716.
(51) Wu, B.; Duncombe, B. J.; Stace, A. J. Unpublished results.